Materials for Quantum Technology

PAPER • OPEN ACCESS

Topological protection of highly entangled non-Gaussian two-photon states

To cite this article: Konrad Tschernig *et al* 2021 *Mater. Quantum. Technol.* **1** 035001

Materials for Quantum Technology

OPEN ACCESS

RECEIVED
23 March 2021

REVISED
2 June 2021

ACCEPTED FOR PUBLICATION
6 July 2021

PUBLISHED
26 July 2021

PAPER

Topological protection of highly entangled non-Gaussian two-photon states

Konrad Tschernig[1,2,*], **Rosario Lo Franco**[3], **Misha Ivanov**[1,2,4], **Miguel A Bandres**[5], **Kurt Busch**[1,2] and **Armando Perez-Leija**[1,2,*]

[1] Max-Born-Institut, Max-Born-Strasse 2A, 12489 Berlin, Germany
[2] Humboldt-Universität zu Berlin, Institut für Physik, AG Theoretische Optik & Photonik, Newtonstrasse 15, 12489 Berlin, Germany
[3] Dipartimento di Ingegneria, Università di Palermo, Viale delle Scienze, Edificio 6, 90128 Palermo, Italy
[4] Blackett Laboratory, Imperial College London, London, United Kingdom
[5] CREOL, The College of Optics and Photonics, University of Central Florida, Orlando, FL 32816-2700, United States of America
[*] Authors to whom any correspondence should be addressed.

E-mail: konrad.tschernig@physik.hu-berlin.de and apleija@gmail.com

Keywords: quantum photonics, topological insulators, two-photon light

Abstract

We study theoretically the evolution of entangled non-Gaussian two-photon states in disordered topological lattices. Specifically, we consider spatially entangled two-photon states, modulated by Laguerre polynomials up to the 3rd order, which feature ring-shaped spatial and spectral correlation patterns. Such states are discrete analogs of photon-subtracted squeezed states, which are ubiquitous in optical quantum information processing or sensing applications. We find that, in general, a higher degree of entanglement coincides with a loss of topological protection against disorder, this is in line with previous results for Gaussian two-photon states. However, we identify a particular regime in the parameter space of the considered non-Gaussian states, where the situation is reversed and an increase of entanglement can be beneficial for the transport of two-photon quantum states through disordered regions.

1. Introduction

In condensed matter physics, topological insulators (TIs) are two-dimensional structures that support single-particle bound states strictly localized at the edges of the system [1]. An intriguing characteristic of such topological edge states is that they are unidirectionally protected against both back-scattering and scattering into the bulk by time-reversal symmetry [2]. As a result, the energy flow in TIs is unidirectional, despite the presence of disorder and defects [3–6].

Inspired by these ideas, it was found that TIs can be achieved in coupled systems provided the couplings between neighboring sites can be appropriately engineered [7, 8]. Thereafter, a plethora of theoretical and experimental investigations have demonstrated how such topological systems can be implemented in numerous physical platforms ranging from quantum wells [9], optical lattices [10], acoustic systems [11], ring resonators [12], and lattice systems in general [13–19].

In the context of optics, photonic topological insulators (PTIs) have been widely studied using waveguide lattices and arrangements of integrated resonators [4, 5, 8, 18–21], and the very existence of scattering-immune states has sparked intensive research aimed to explore their applicability as quantum channels in which the transport of multiphoton entanglement is topologically protected [22–25]. Recent work [26] has highlighted the precise prescription to implement the spatial and spectral correlations of Gaussian two-photon states, as otherwise the topological protection offered by PTIs would be severely limited. Specifically, in [26] is demonstrated that increasing the amount of entanglement yields to a faster deterioration of two-photon Gaussian states after propagation through disordered systems. Beyond Gaussian states, here, we analyze the impact of disorder on non-Gaussian [27] two-photon states traveling on PTIs. Importantly, non-Gaussian states may exhibit higher a degree of entanglement than their Gaussian counterparts [28] and for this reason they constitute an appealing resource for applications in quantum optical information processing [29, 30]

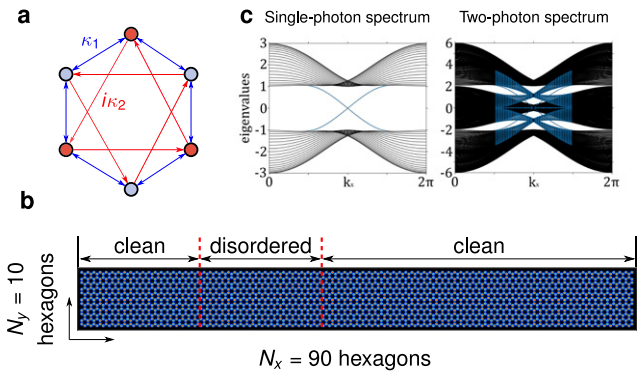

Figure 1. Haldane TI lattice. (a) Hexagonal cell of the Haldane lattice. In our simulations, we set the real-valued nearest-neighbor coupling coefficient $\kappa_1 = 1$ (blue arrows). The next-nearest-neighbor coupling (red arrows) is complex-valued, with $i\kappa_2$ in the direction of the arrows and $-i\kappa_2$ in the opposite direction and we set $\kappa_2 = 0.2$. (b) Finite lattice used in our simulations with $N_x = 90$ hexagons in the x-direction and $N_y = 10$ hexagons in y-direction. For our scattering analyses, we introduce disorder to the on-site energies in the region sandwiched between the two red vertical lines. (c) (Left panel) single-photon and two-photon (right panel) band structures of a semi-infinite strip.

and sensing [31]. It is thus of high interest to investigate the possibility of topologically-protected transport of highly-entangled non-Gaussian states.

2. Results

In contrast to two-photon Gaussian states, for non-Gaussian entangled states, we have identified a regime in parameter space where increasing the amount of entanglement becomes beneficial for the transport of the states. For the sake of concreteness, we perform our analysis using a Haldane topological lattice system [32], which in optics can be implemented using a photonic honeycomb lattice composed of helical waveguides (see reference [8] for details). Note, in the photonic context of Haldane lattices the time t is replaced by the propagation distance z, that is, the time evolution occurs along the propagation direction. Further, we consider that every waveguide in a hexagonal cell exhibits a nearest neighbor coupling $\kappa_1 = 1$, while the next nearest neighbor coupling is complex-valued $\kappa_2 = i\kappa_1/5$, figure 1(a). Throughout this work we use normalized units. At the single-photon level such a Haldane lattice is described by the Hamiltonian

$$\hat{H} = \kappa_1 \sum_{\langle i,j \rangle} \left(\hat{a}_i^\dagger \hat{a}_j + \hat{a}_j^\dagger \hat{a}_i \right) + i\kappa_2 \sum_{\langle\langle i,j \rangle\rangle} \left(\hat{a}_i^\dagger \hat{a}_j - \hat{a}_j^\dagger \hat{a}_i \right), \tag{1}$$

where the optical mode in the ith site is represented by the creation (annihilation) operator, $\hat{a}_i^\dagger$ ($\hat{a}_i$). That is, the action of $\hat{a}_i^\dagger$ ($\hat{a}_i$) on the vacuum state $|0\rangle$ creates (annihilates) a photon in site i, $\hat{a}_i^\dagger |0_i\rangle = |1_i\rangle$ $\left(\hat{a}_i |1_i\rangle = |0_i\rangle\right)$. Moreover, the symbols $\langle\rangle$ and $\langle\langle\rangle\rangle$ indicate summation over nearest and next-nearest neighbor sites, respectively.

Before discussing disordered PTIs, it is elucidating to compare the band structures arising in a hypothetical infinitely long TI-strip excited by a single photon and by two photons. In the single-photon case, the band structure exhibits topological edge states residing in the bulk gap as illustrated in the left panel of figure 1(c). In contrast, for two indistinguishable photons, the emerging band structure does not present any gap, see right panel in figure 1(c). Therefore, it is not immediately obvious that two-photon states are topologically protected. However, two-photon states can be protected just as well as single-photon states, provided the joint spectral correlation map of the photons lies inside the so-called topological window of protection [26].

In agreement with the symmetrization postulate of quantum mechanics [33], the absence of the bulk gap can be explained from the fact that for two indistinguishable noninteracting bosons, the Hamiltonian is given as $\hat{H}^{(2)} = \hat{H} \otimes \hat{I} + \hat{I} \otimes \hat{H}$, where $\hat{H}$ is the single-particle Hamiltonian and $\hat{I}$ is the identity matrix of the same dimensions. Due to the symmetric structure exhibited by $\hat{H}^{(2)}$ it is not difficult to see that the two-photon eigenstates are given by the symmetric tensor-product combinations of the single-photon eigenstates

$$|\phi_{p,q}^{(2)}\rangle = \begin{cases} |\phi_p\rangle \otimes |\phi_q\rangle \Leftrightarrow p = q, \\ \dfrac{1}{\sqrt{2}} \left(|\phi_p\rangle \otimes |\phi_q\rangle + |\phi_q\rangle \otimes |\phi_p\rangle \right) \Leftrightarrow p \neq q, \end{cases} \tag{2}$$

and the two-photon eigenvalues are the sums of the corresponding single-photon eigenvalues $\lambda_{p,q}^{(2)} = \lambda_p + \lambda_q$. Notice, λ_p and λ_q represent the single-photon eigenvalues corresponding to the pth and qth single-photon

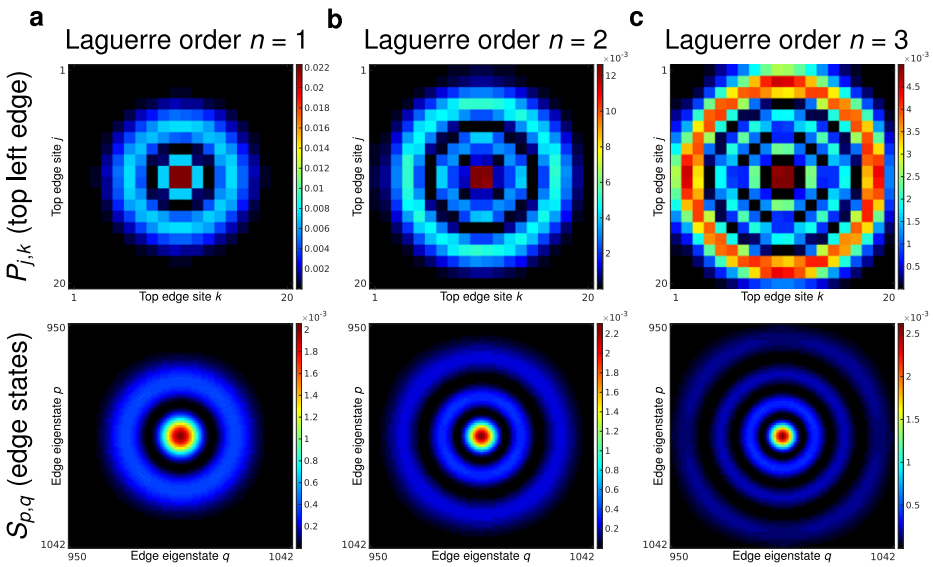

Figure 2. Spatial correlation maps $P_{j,k}$ and spectral correlation maps $S_{p,q}$ of non-Gaussian entangled two-photon topological edge states, with $\sigma_G = \sigma_L = 2.5$. (a)–(c) Laguerre polynomial of order $n = 1, 2, 3$, respectively. All states feature a central lobe in both $P_{j,k}$ and $S_{p,q}$. Additionally, we observe n concentric correlation 'rings' around the central lobe, and their number also indicates the degree of entanglement of the states. Specifically, the states feature a Schmidt number $K = 1.99, 2.89, 3.71$ for $n = 1, 2, 3$ respectively. Note that by carefully tuning σ_G and σ_L it is possible to achieve states with Schmidt numbers arbitrarily close to the maximum amount of entanglement allowed by the order of the Laguerre polynomial $K \lesssim n + 1$.

eigenmodes, $|\phi_p\rangle$ and $|\phi_q\rangle$. For the lattice used here, the single-photon edge subspace comprises the eigenmodes $\mathcal{E} = \{|\phi_n\rangle : 950 \leqslant n \leqslant 1042\}$, while the rest are bulk-modes $\mathcal{B}$. This allows us to split the two-photon eigenspace into three disjoint subspaces—bulk–bulk $\mathcal{B} \otimes \mathcal{B}$, bulk–edge $\mathcal{B} \otimes \mathcal{E}$ and edge–edge $\mathcal{E} \otimes \mathcal{E}$. In the appendix A we describe how to identify the edge eigenmodes.

We now turn our attention to analyze the effects of disorder on two-photon states. To do so, we consider a finite Haldane honeycomb lattice containing three regions as depicted in figure 1(b). The left and right regions of the lattice are disorder-free, that is, the refractive indices of all these sites are equal, which implies that all the propagation constants are equal, i.e. $\beta_j = 0$. In the intermediate part we introduce static diagonal disorder, that is, disorder in the on-site refractive index. Specifically, the individual propagation constants β_j for each site of the disordered region are taken randomly from a normal distribution with mean $\mu = 0$ and variance $\sigma = 1$. In order to exclude strong outliers, we truncate the distribution such that $|\beta_j| \leqslant \sqrt{2}$ is fulfilled for all sites in the disordered region. It is important to stress that these values of β_j ensure that the disorder is weak enough to not destroy topological protection (e.g. by closing the bandgap) for single photons, because the disorder strength as defined by the variance $\sigma = 1$ is smaller than the bulk bandgap $\Delta \approx 2$.

To generate non-Gaussian entangled states, we start with the expression

$$|\tilde{\psi}^{(2)}_{\sigma_G,\sigma_L,n}\rangle = \sum_{j,k=1}^{M_e} (-1)^{j+k}\, e^{-\frac{(j-x_0)^2+(k-x_0)^2}{2\sigma_G^2}}\, L_n\left(\frac{(j-x_0)^2+(k-x_0)^2}{\sigma_L^2}\right)|1_j, 1_k\rangle, \tag{3}$$

where j, k are the waveguide indices of the first $M_e = 20$ sites on the top edge of the lattice, $x_0 = (M_e + 1)/2$ is the spatial center in this range, and $|1_j, 1_k\rangle$ corresponds to the two-photon-state describing a photon at site j and its twin photon at site k. The width of the Gaussian envelope is controlled by σ_G (Gaussian width), and the modulating function is the Laguerre-polynomial $L_n(x)$ of order n, controlled by σ_L (Laguerre width).

To ensure that solely edge states will be present in the initial states we project the spatial state given in equation (3) onto the two-photon eigenstates $|\phi^{(2)}_{p,q}\rangle$, and then remove the components belonging to the subspaces $\mathcal{B} \otimes \mathcal{E}$ and $\mathcal{B} \otimes \mathcal{B}$. In that way we obtain the spectral representation of the non-Gaussian two-photon states comprising only edge states

$$|\psi^{(2)}_{\sigma_G,\sigma_L,n}\rangle = \frac{1}{A}\sum_{p,q}^{\mathcal{E}\otimes\mathcal{E}} \sum_{j,k=1}^{M_e} \psi_{j,k}\langle\phi^{(2)}_{p,q}|1_j, 1_k\rangle|\phi^{(2)}_{p,q}\rangle, \tag{4}$$

where A is the normalization constant, and $\psi_{j,k}$ are the coefficients appearing in equation (3). The spectral and spatial correlation maps corresponding to these states are easily computed via $S_{p,q} = |\langle\phi^{(2)}_{p,q}|\psi^{(2)}_{\sigma_G,\sigma_L,n}\rangle|^2$, and $P_{j,k} = |\langle 1_j, 1_k|\psi^{(2)}_{\sigma_G,\sigma_L,n}\rangle|^2$, respectively. In figure 2 we show some exemplary states for $\sigma_G = \sigma_L = 2.5$ and

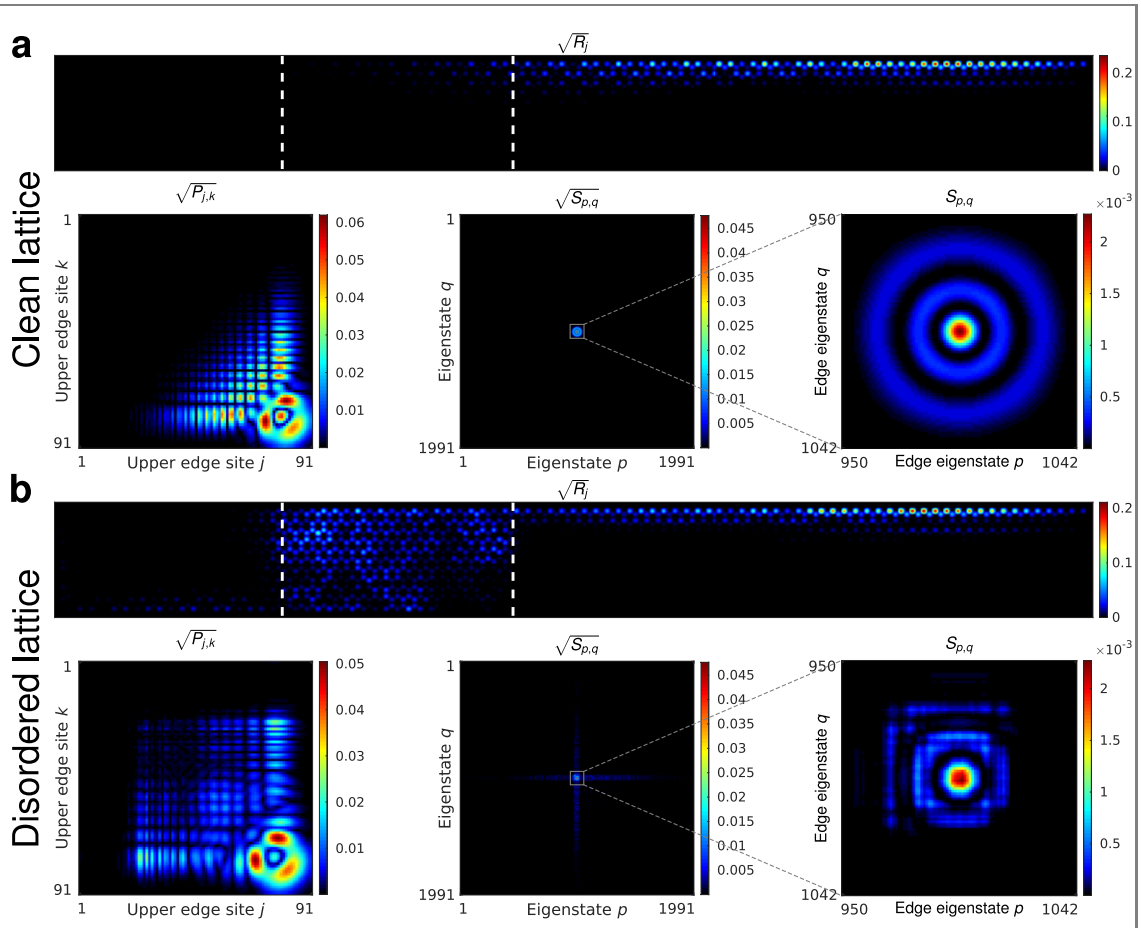

Figure 3. Evolved second-order non-Gaussian entangled state $|\psi^{(2)}_{\sigma_G=\sigma_L=2.5,n=2}\rangle$ after a propagation distance $z = 75$. (a) and (b) correspond to the completely clean system and to the system with disorder, respectively. In both cases we show the evolved spatial marginal distribution R_j (top)—where the dashed lines indicate the region with disorder—the spatial correlation map on the sites of the upper edge $P_{j,k}$ (bottom left) and the spectral correlation map $S_{p,q}$ (middle: complete eigenspace, right: magnified edge–edge subspace). In order to improve the visibility of small amplitudes, we plot, in some cases, the square root as indicated.

$n = 1, 2, 3$. All these states feature a central lobe surrounded by n concentric rings in both the spectral and spatial correlation maps. These rings—and their number—effectively encode the degree of entanglement of the states, since the Schmidt number K of the corresponding states is in general close to $n + 1$. Note that we define the Schmidt number in the usual way [34]

$$K = \left[\sum_{m=1}^{M} k_m^2\right]^{-1}, \tag{5}$$

where k_m are the Schmidt amplitudes obtained from the singular value decomposition of the reduced density matrix $\hat{\rho}_{\text{red}} = \text{Tr}\left(|\psi^{(2)}_{\sigma_G,\sigma_L,n}\rangle\langle\psi^{(2)}_{\sigma_G,\sigma_L,n}|\right)$ where the trace runs over the eigenstates of one of the photons. Explicitly, for the states shown in figure 2, $K_{n=1,2,3} = 1.99, 2.89, 3.71$, which certifies their entanglement [35]. Analogous results about entanglement characterization of the edge states of equation (4) can be obtained by the Schmidt decomposition within the no-label approach as described in references [36, 37].

We now proceed to study the evolution of these states through the disordered region of the lattice. As an example, we show the evolution of the second-order state $|\psi^{(2)}_{\sigma_G=2.5=\sigma_L,n=2}\rangle$ in the clean lattice, figure 3(a), and in the disordered lattice, figure 3(b). In the presence of disorder a significant part of the two-photon state is scattered into the bulk, which can be seen in the spatial marginal distribution $R_j = \sum_{k=1}^{M} P_{j,k}$ as well as in the spectral correlation maps. A close inspection of the correlation map computed after the disordered region, one sees that mainly the outer spectral correlation ring is affected the most by the disorder (see leftmost figure in the lower row of figure 3(b)). This is in line with previous results—the two-photon spectral amplitudes outside of the topological window of protection are scattered away from the edge [26]. In this specific case only the center lobe and the inner correlation ring fit inside the window of protection.

In order to quantify the degree of topological protection, we consider two figures of merit. Firstly, we compute the transmittance $T = \sum_{j,k} P_{j,k}$, where the sum runs over the sites j, k located to the right-hand side of

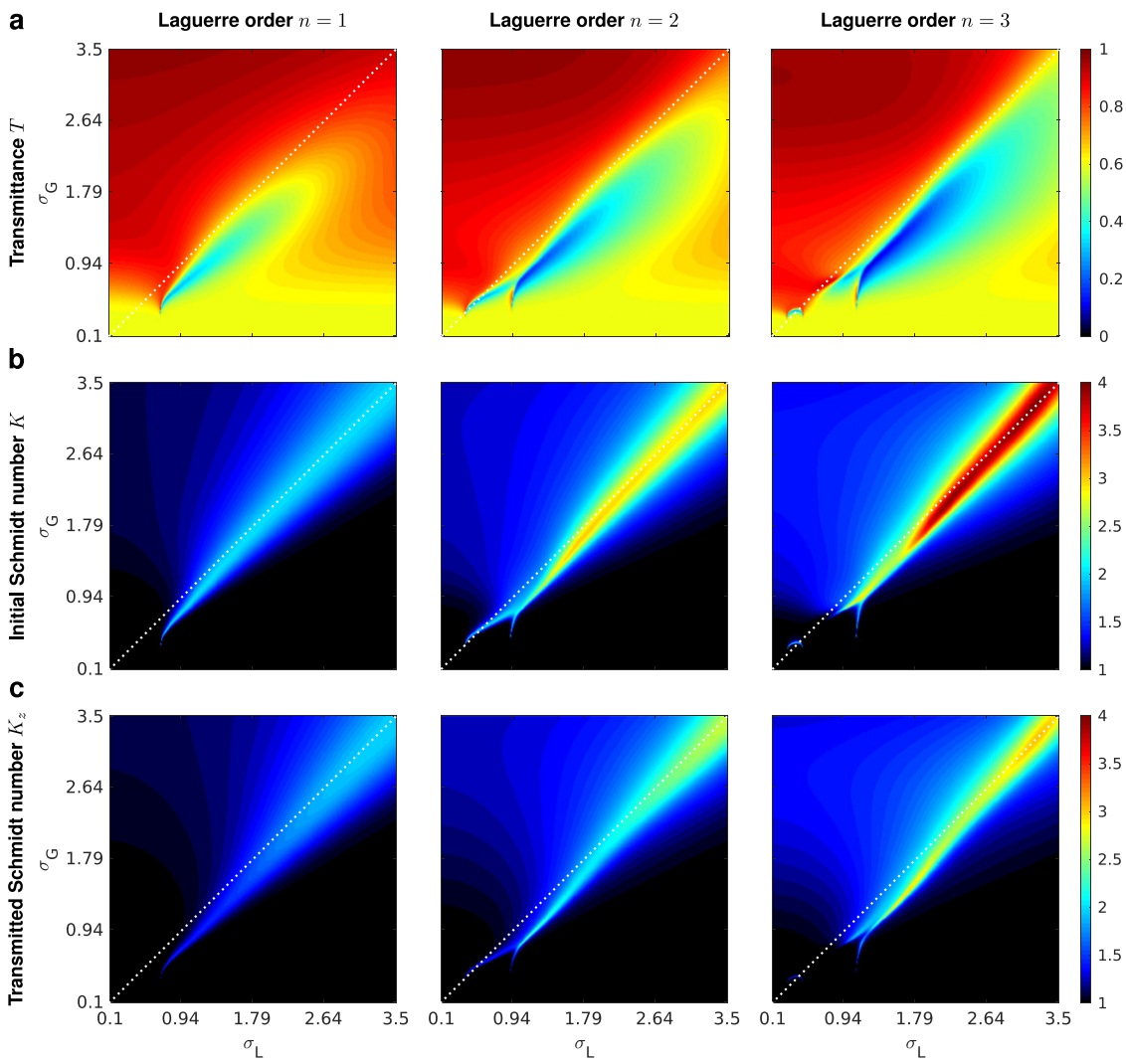

Figure 4. (a) Transmittance T, (b) initial Schmidt number K and (c) final Schmidt number K_z of the states $|\psi^{(2)}_{\sigma_G,\sigma_L,n}\rangle$ after propagation through the disordered region. The three columns correspond to the order $n = 1, 2, 3$ of the modulating Laguerre polynomials, respectively. In each case we have performed a scan over the Gaussian width $\sigma_G \in [0.1, 3.5]$ and the Laguerre width $\sigma_L \in [0.1, 3.5]$. Additionally, we have performed these parameter scans for 20 different instances of the random disorder and show here the ensemble average.

the disordered region. Physically, T represents the amount of probability transmitted through the disordered region without scattering into the bulk. Secondly, we estimate the Schmidt number K_z of the transmitted state. To do so, we first calculate the reduced density matrix of the evolved state $\hat{\rho}_{\text{red}}(z) = \text{Tr}_1\left(|\psi^{(2)}(z)\rangle\langle|\psi^{(2)}(z)\rangle|\right)$. Then we project the reduced state onto the spatial region to the right-hand-side of the disordered region $\hat{\rho}_{\text{red,proj}} = \frac{1}{A}\sum_{j,k}|1_j\rangle\langle 1_j|\hat{\rho}_{\text{red}}|1_k\rangle\langle 1_k|$, where A is a renormalization constant such that $\text{Tr}\left(\hat{\rho}_{\text{red,proj}}\right) = 1$. The Schmidt amplitudes k_m of $\hat{\rho}_{\text{red,proj}}$ are then used to compute the Schmidt number K_z of the transmitted state according to equation (5). Therefore, K_z encodes the amount of entanglement in the transmitted two-photon state, the results are summarized in figure 4. The plots of the transmittance, figure 4(a), show that in general the states lying above the diagonal dashed line ($\sigma_G > \sigma_L$) are protected to a higher degree than those appearing below it ($\sigma_G < \sigma_L$). The reason is that broadening the Gaussian envelope of the initial states implies a larger spatial extension, this in turn leads to a narrowing in the corresponding spectrum such that the states become more confined into the protection window. In all cases, the initial states exhibiting the highest degree of entanglement are mainly located on the diagonal $\sigma_G = \sigma_L$ (dotted lines). As a consequence, the highest protected entanglement K_z is also found along the diagonal and toward the top right corners, where σ_G and σ_L take on their largest values in the range displayed. In the regions below the diagonal appear some intriguing features, where the transmittance and the protected entanglement can vary rapidly with small changes of σ_G and σ_L.

To investigate this peculiar behavior, we now take a closer look at the specific case $n = 1$, $\sigma_L = 0.708$, figure 5. As one can see, the transmittance exhibits a local minimum $\sigma_{G_{\text{min}}} = 0.357$, $T = 0.285$ and a local maximum $\sigma_{G_{\text{max}}} = 0.404$, $T = 0.818$ for a change of $\delta_G = \sigma_{G_{\text{max}}} - \sigma_{G_{\text{min}}} \approx 0.05$ in the Gaussian width of the states. In between, the Schmidt number of the evolved states reaches a local maximum at $\sigma_{G_K} = 0.361$,

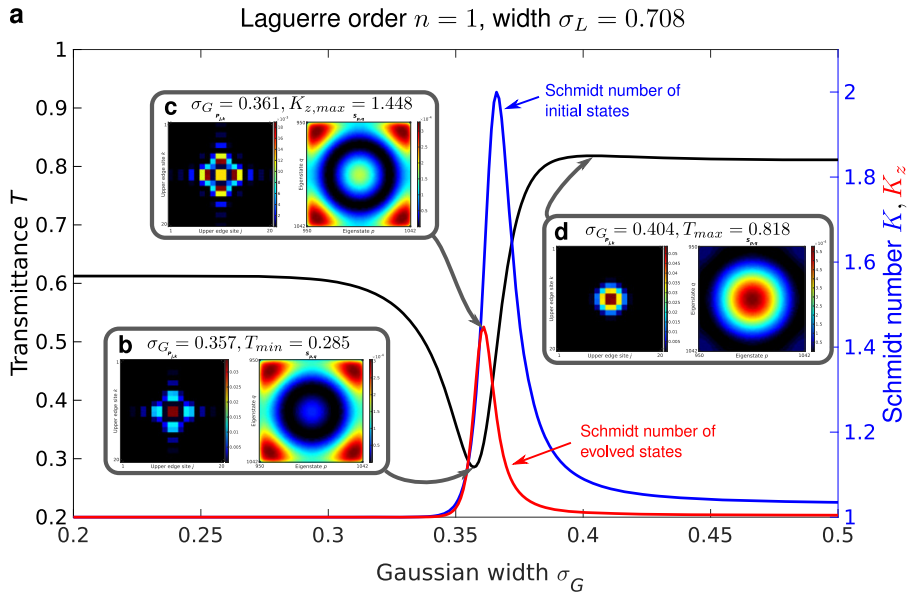

Figure 5. Rapid oscillations of the transmission and protected entanglement. (a) Plot of the transmittance T (black line), initial Schmidt number K (blue lines) and the transmitted Schmidt number K_z (red line) of the states with $\sigma_L = 0.708$, $n = 1$ and $\sigma_G \in [0.25, 0.5]$. In the insets we show the spatial and spectral correlation maps of the states with: (b) the smallest T ($\sigma_G = 0.357$), (c) the largest K_z ($\sigma_G = 0.361$), (d) the largest T ($\sigma_G = 0.404$).

$K_z = 1.448$. The corresponding initial states are visualized in figures 5(b)–(d). Interestingly, the state for which T is a minimum, figure 5(b), features a strongly localized central spatial correlation lobe. Concurrently, this state lacks the central spectral correlation lobe as previously observed in figure 2. This is clearly the reason for its lack of topological protection since almost all of its spectral correlations lie outside of the protection window. As σ_G increases, the transmittance T and the entanglement K_z grow simultaneously until we reach the state shown in figure 5(c). In a reversed fashion, compared to the state in figure 5(b), now the spatial correlation lobe is suppressed, while the spectral correlation lobe reappears. The reappearance of the central spectral lobe ultimately grants this state (σ_{G_K}) a higher degree of protection than its less entangled partner state ($\sigma_{G_{min}}$). To the best of our knowledge, this continuous progression of states, where the Gaussian width passes from $\sigma_G = 0.357$ to $\sigma_G = 0.361$ ($\sigma_L = 0.708, n = 1$), is the first example where an increment in entanglement improves the topological protection of two-photon states. However, any further increase in σ_G reduces the amount of protected entanglement until the resulting states resemble uncorrelated product states, figure 5(d). Note, that very similar behavior can be observed also for other parameter choices of the Laguerre width σ_L and order n, as illustrated in figure 4. An interesting question arises as to whether these phenomena can also be observed when—in addition to the disorder—also some sites of the lattice are completely absent. As we describe in the appendix A, we have performed some simulations akin to the ones shown in figure 5 for a system in which some sites in a spatial section on the upper edge in the disordered region have been removed. Apart from a slight reduction in the transmission T and final Schmidt number K_z, we observe identical behavior as seen in figure 5. Therefore, also the removal of several edge-sites does not significantly reduce the topological protection.

At this point we briefly outline a possible way to generate the non-Gaussian states considered here and address the potential challenges for experimental observations of these effects. Two-photon states can be generated using standard spontaneous-parametric-down-conversion nonlinear crystals. Using a positive achromatic doublet lens [38], it is then possible to project an image of the crystal output onto a spatial-light-modulator, which in turn can be programmed to apply suitable phase and amplitude modifications to the incoming two-photon wavefronts. Then, using another lens one can couple the two-photon states into the sites of the upper edge of the waveguide lattice. Another possibility is to use a discrete fractional Fourier lattices to tailor the correlations of the photons emerging from the nonlinear crystal [39, 40].

Before concluding, we address the role of particle indistinguishability in the topological protection. Since we are considering non-interacting particles, one may think, that the two-photon evolution is ruled completely by the single particle dynamics. However, we cannot simply consider the photons separately: in general, the reduced single particle states (where one of the photons is disregarded or traced out) are mixed states and, as a result, the dynamics will be similar to the one exhibited by partially coherent light [41]. At this point it is worth to stress that topological protection of a two-photon state is a fully coherent effect and partial coherence will definitely prevent its observation. This point can be shown more prominently by considering the most

extreme case of a maximally entangled two-photon state of the form $|\psi\rangle = \sum_m \psi_m |1_m, 1_m\rangle$, whose reduced density operator is completely incoherent, $\hat{\rho}_{\mathrm{red}} = \sum_m |\psi_m|^2 |1_m\rangle\langle 1_m|$. Further, introducing disorder or dephasing into the system will increase the incoherence of the reduced single-particle states. In realistic scenarios, incoherent effects might come from defects or random modifications in the photonic structures that render the evolution in these systems to be non-unitary and, as a result, the states will undergo dephasing. Thus, each product state (or Schmidt mode) in a superposition that forms the entangled state will acquire random phases, leading to dephasing of the superposition and the loss of entanglement, even if each product state on its own is protected. Consequently, in order to reduce the impact of these effects—and to observe two-photon topological protection—a high degree of indistinguishability among the photon pair is of paramount importance. We point out that these arguments also find support in previous results where the degree of indistinguishability of identical particles has been shown to shield quantum entanglement against both non-dissipative and dissipative noise channels [42, 43]. Moreover, it has been recently demonstrated experimentally that two-photon quantum correlations in a quantum walk network can be enhanced under disordered dynamics thanks to the indistinguishability of the photons [44, 45].

3. Conclusions

In summary, we have shown that non-Gaussian entangled two-photon states can be topologically protected, provided their joint-spectral correlation function is well-confined to the topological window of protection. This is achieved with the choice $\sigma_{\mathrm{G}} \approx \sigma_{\mathrm{L}}$, i.e. the spatial extent of the Gaussian envelope and the modulating function are approximately identical and—importantly—large enough. The resulting states maintain their spectral correlation pattern even in the presence of disorder, which renders them an appealing resource for applications in quantum optical information processing. In this regard it is known that quantum random walk-based algorithms are a possible platform for efficient quantum computations [46]. Quantum random walks along the edges of PTIs might provide significant advantages, since the walker's dynamics would be protected against disorder, such as fabrication errors—intrinsically. Furthermore, we identify a regime in the parameter space, where an increase in the degree of entanglement can improve the protection against disorder. This surprising result may serve as a starting point for further investigations into the engineering of useful entangled states in PTI systems.

Acknowledgments

KT, APL, and KB acknowledge support by the Deutsche Forschungsgemeinschaft (DFG) within the framework of the DFG priority program 1839 Tailored Disorder (BU 1107/12-2, PE 2602/2-2). MI acknowledges funding from the European Union's Horizon 2020 research and innovation programme under Grant Agreement No. 899794.

Data availability statement

The data generated and/or analysed during the current study are not publicly available for legal/ethical reasons but are available from the corresponding author on reasonable request.

Appendix A.

A.1. Identification of the edge modes

We start by calculating the complete set of single-particle eigenmodes $|\phi_n\rangle$ of the finite Haldane lattice. Next, we sort the eigenmodes $|\phi_n\rangle$ according to their eigenvalues λ_n in ascending order, as shown in figure 6(a). Now we calculate for each eigenmode $|\phi_n\rangle$ the edge intensity

$$I_n = \sum_j |\langle j|\phi_n\rangle|^2, \tag{A.6}$$

where the sum runs only over the sites j on the outer-most spatial edge of the finite lattice. In figure 6(b) we observe a distinct spectral region where the edge intensity is significantly enhanced. However, in order to reliably identify the edge-modes we calculate the differential edge intensity $\Delta I_n = I_{n+1} - I_n$ in figure 6(c). Here we observe a global maximum $\Delta I_{949} \approx 0.26$ and a global minimum$\Delta I_{1042} \approx -0.26$. Thus we can identify the

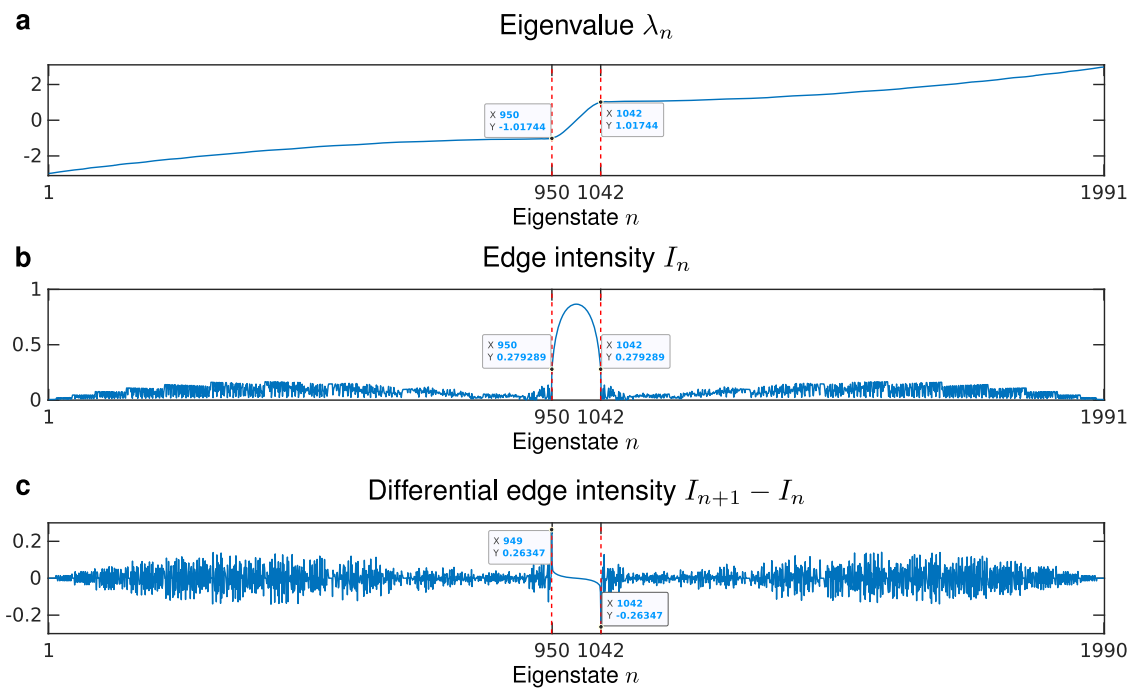

Figure 6. Process of identification of the edge and bulk modes of the Haldane lattice. (a) We sort the eigenmodes according to their eigenvalues in ascending order and (b) calculate the edge intensity of each eigenmode. (c) The edge subspace is obtained by identifying the global minimum and maximum of the differential edge mode intensity $\Delta I_n = I_{n+1} - I_n$.

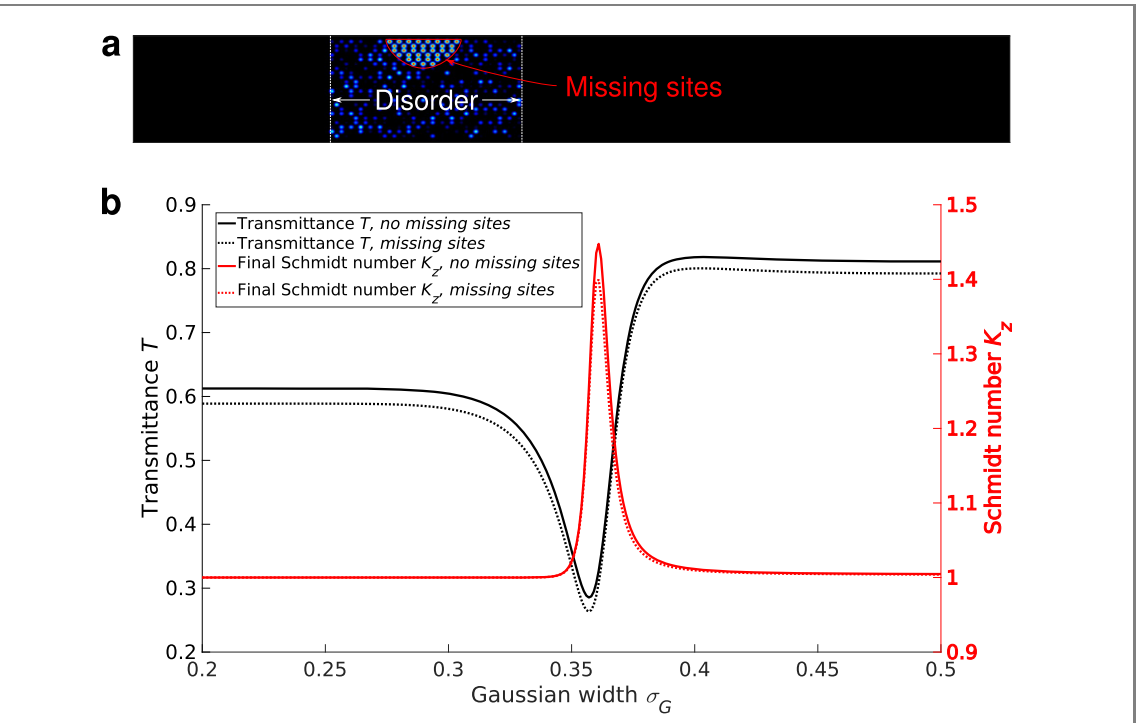

Figure 7. (a) In the disordered region we remove the sites on the top edge as indicated. (b) The resulting transmittance T (black lines) and final Schmidt number (red lines) are slightly reduced (dotted lines) with respect to the case where no sites are missing (solid lines). The parameter-range considered here is the same as in figure 5 ($n = 1, \sigma_L = 0.708$).

edge mode subspace in the following way

$$\mathcal{E} = \{|\phi_n\rangle : 950 \leqslant n \leqslant 1042\}\,, \tag{A.7}$$

and all other eigenstates belong to the bulk mode subspace

$$\mathcal{B} = \{|\phi_n\rangle : 950 > n > 1042\}\,. \tag{A.8}$$

A.2. Impact of missing sites

We consider the case where in addition to disorder also several sites on the top edge are removed. Now, the two-photon wavefunctions are traveling along a new edge as indicated in figure 7(a). In order to gauge the impact of the removal of these sites, we perform the same analysis as was done in figure 5. Our results show, figure 7(b), that the key figures of merit—the transmission and final Schmidt number—are only slightly reduced with respect to the case where all sites are present. Thus, we conclude that the topological protection of non-Gaussian states holds also for these kinds of defects.

ORCID iDs

Konrad Tschernig https://orcid.org/0000-0003-0035-2703
Rosario Lo Franco https://orcid.org/0000-0002-3281-0935
Misha Ivanov https://orcid.org/0000-0002-8817-2469
Miguel A Bandres https://orcid.org/0000-0002-7145-8567
Kurt Busch https://orcid.org/0000-0003-0076-8522
Armando Perez-Leija https://orcid.org/0000-0002-6218-295X

References

[1] Bernevig A-B and Hughes T-L 2013 *Topological Insulators and Topological Superconductors* (Princeton, NJ: Princeton University Press)
[2] Piatrusha S U, Tikhonov E S, Kvon Z D, Mikhailov N N, Dvoretsky S A and Khrapai V S 2019 *Phys. Rev. Lett.* **123** 056801
[3] Wang Z, Chong Y D, Joannopoulos J D and Soljačić M 2008 *Phys. Rev. Lett.* **100** 013905
[4] Lu L, Joannopoulos J D and Soljačić M 2014 *Nat. Photon.* **8** 821
[5] Khanikaev A B, Hossein Mousavi S, Tse W-K, Kargarian M, MacDonald A H and Shvets G 2013 *Nat. Mater.* **12** 233
[6] Wang Z, Chong Y, Joannopoulos J D and Soljačić M 2009 *Nature* **461** 772
[7] Haldane F D M and Raghu S 2008 *Phys. Rev. Lett.* **100** 013904
[8] Rechtsman M C, Zeuner J M, Plotnik Y, Lumer Y, Podolsky D, Dreisow F, Nolte S, Segev M and Szameit A 2013 *Nature* **496** 196
[9] Bernevig B A, Hughes T L and Zhang S-C 2006 *Science* **314** 1757
[10] Tarruell L, Greif D, Uehlinger T, Jotzu G and Esslinger T 2012 *Nature* **483** 302
[11] Yang Z, Gao F, Shi X, Lin X, Gao Z, Chong Y and Zhang B 2015 *Phys. Rev. Lett.* **114** 114301
[12] Liu Y G N, Jung P S, Parto M, Christodoulides D N and Khajavikhan M 2021 *Nat. Phys.* **17** 704
[13] Bomantara R W, Zhou L, Pan J and Gong J 2019 *Phys. Rev.* B **99** 045441
[14] Volpez Y, Loss D and Klinovaja J 2017 *Phys. Rev.* B **96** 085422
[15] Seiberg N and Witten E 2016 *Prog. Theor. Exp. Phys.* **2016** 12C101
[16] Stanescu T D, Galitski V, Vaishnav J Y, Clark C W and Das Sarma S 2009 *Phys. Rev.* A **79** 053639
[17] Jotzu G, Messer M, Desbuquois R, Lebrat M, Uehlinger T, Greif D and Esslinger T 2014 *Nature* **515** 237
[18] Lustig E, Weimann S, Plotnik Y, Lumer Y, Bandres M A, Szameit A and Segev M 2019 *Nature* **567** 356
[19] Slobozhanyuk A, Mousavi S H, Ni X, Smirnova D, Kivshar Y S and Khanikaev A B 2017 *Nat. Photon.* **11** 130
[20] Wen-Jie C, Shao-Ji J, Xiao-Dong C, Baocheng Z, Lei Z, Jian-Wen D and Chan C T 2014 *Nat. Commun.* **5** 5782
[21] Cheng X, Jouvaud C, Ni X, Mousavi S H, Genack A Z and Khanikaev A B 2016 *Nat. Mater.* **15** 542
[22] Mittal S, Orre V V and Hafezi M 2016 *Opt. Express* **24** 15631
[23] Rechtsman M C, Lumer Y, Plotnik Y, Perez-Leija A, Szameit A and Segev M 2016 *Optica* **3** 925
[24] Blanco-Redondo A, Bell B, Oren D, Eggleton B J and Segev M 2018 *Science* **362** 568
[25] Michelle W, Cooper D, Bryn B, Eric M, Mordechai S and Andrea B-R 2019 *Topologically Protected Entangled Photonic States* vol 8 (Berlin: de Gruyter & Co) pp 1327–8
[26] Tschernig K, Jimenez-Galán Á, Christodoulides D N, Ivanov M, Busch K, Bandres M A and Perez-Leija A 2021 *Nat. Commun.* **12** 1974
[27] Lvovsky A I, Grangier P, Ourjoumtsev A, Parigi V, Sasaki M and Tualle-Brouri R 2020 arXiv:2006.16985
[28] Walschaers M, Parigi V and Treps N 2020 *PRX Quantum* **1** 020305
[29] Genoni M G and Paris M G A 2010 *Phys. Rev.* A **82** 052341
[30] Seshadreesan K P, Dowling J P and Agarwal G S 2015 *Phys. Scr.* **90** 074029
[31] Dowling J P 2008 *Contemp. Phys.* **49** 125
[32] Haldane F D M 1988 *Phys. Rev. Lett.* **61** 2015
[33] Tschernig K, Muller C, Smoor M, Kroh T, Wolters J, Benson O, Busch K and Perez-Leija A 2020 arXiv:2011.08777
[34] Sperling J and Vogel W 2011 *Phys. Scr.* **83** 045002
[35] Sperling J, Perez-Leija A, Busch K and Silberhorn C 2019 *Phys. Rev.* A **100** 062129
[36] Sciara S, Lo Franco R and Compagno G 2017 *Sci. Rep.* **7** 44675
[37] Lo Franco R and Compagno G 2016 *Sci. Rep.* **6** 20603
[38] Di Giuseppe G *et al* 2013 *Phys. Rev. Lett.* **110** 150503
[39] Perez-Leija A, Keil R, Moya-Cessa H, Szameit A and Christodoulides D N 2013 *Phys. Rev.* A **87** 022303
[40] Weimann S *et al* 2016 *Nat. Commun.* **7** 11027
[41] Abouraddy A F, Saleh B E A, Sergienko A V and Teich M C 2001 *Phys. Rev. Lett.* **87** 123602
[42] Nosrati F, Castellini A, Compagno G and Lo Franco R 2020 *npj Quantum Inf.* **6** 39

[43] Nosrati F, Castellini A, Compagno G and Lo Franco R 2020 *Phys. Rev.* A **102** 062429
[44] Perez-Leija A, Guzmán-Silva D, León-Montiel R d J, Gräfe M, Heinrich M, Moya-Cessa H, Busch K and Szameit A 2018 *npj Quantum Inf.* **4** 45
[45] Laneve A, Nosrati F, Geraldi A, Mahdavipour K, Pegoraro F, Khazaei-Shadfar M, Lo Franco R and Mataloni P 2020 arXiv:2102.04755
[46] Kempe J 2003 *Contemp. Phys.* **44** 307